Phase-matched gratings for enhanced forward degenerate four-wave mixing

E. Giorgetti

Instituto di Ricerca sulle Onde Elettromagnetiche IROE, Consiglio Nazionale delle Ricerche, Via Panciatichi 64, 50127 Firenze, Italy

P. Lambkin

Department of Pure and Applied Physics, Trinity College, University of Dublin, Dublin 2, Ireland

Qu Li

Shanghai Jiao Tong University, 1945 Hua Shan Road, 200030 Shanghai, China

L. Palchetti and S. Sottini

Instituto di Ricerca sulle Onde Elettromagnetiche IROE, Consiglio Nazionale delle Ricerche, Via Panciatichi 64, 50127 Firenze, Italy

D. Grando

Politecnico di Bari, Via Orabona 4, 70125 Bari, Italy

W. Blau

Department of Pure and Applied Physics, Trinity College, University of Dublin, Dublin 2, Ireland

Received May 10, 1994; accepted July 26, 1994; revised manuscript received August 18, 1994

A phase-matched grating to enhance the second-order diffracted signals generated by forward degenerate four-wave mixing has been proposed and demonstrated for the first time to the authors' knowledge. Experiments have been performed with a cw Ar:Kr laser at $\lambda = 488$ nm, with a linear–nonlinear sandwich of glass slides and Alizarin Yellow-doped films of epoxy resin. Finite-difference simulations have been used to model the process successfully, with finite beam size effects and deviations from an ideal Kerr response of the material taken into account. The possibilities for optical processing applications are assessed in the light of these results.

1. INTRODUCTION

The coupling between electromagnetic waves propagating in a nonlinear medium gives rise to a number of interesting phenomena. Specifically, the transfer of energy between two interfering laser beams (two-wave mixing) and the subsequent generation of new beams (four-wave mixing) has been demonstrated in a wide class of materials.[1,2] Photorefractive crystals have been studied in detail with regard to such effects.[3,4] Closely related, at least formally, are materials characterized by the Kerr effect. In these media the refractive index is governed by the following relationship:

$$n = n_0 + n_2 I\,, \tag{1}$$

where I is the local electric field intensity, n_0 is the background index, and n_2 is the nonlinear index. When two coherent pump waves intersect at a narrow angle in such a medium, the resulting interference pattern perturbs the local refractive index and produces a grating. The writing beams scatter from the grating and can generate new diffracted beams. This process is known as forward degenerate four-wave mixing. The pitch of the induced grating is such that the angle of incidence for each writing beam is also the Bragg angle for the grating. As a result, the first-order diffracted beam from each pump appears in the path of the other. The strongest spatially distinguishable order will therefore be the second, and it is these waves that are of primary interest here.

The second-order diffracted beams are not phase matched over significant propagation distances, and so the energy associated with these orders is small. However, by introducing linear spacer layers into the nonlinear medium one can form a grating of gratings. This permits some degree of phase matching, thus enhancing the diffracted sidelobes. This concept is not dissimilar to that proposed for stratified volume holographic elements in which interfering beams would write a permanent grating into thin layers of holographic material separated

0740-3224/95/010058-09$06.00

by homogeneous buffer layers. Such a structure is predicted to exhibit unique diffraction properties as well as those obtained from standard volume holograms.[5–7]

Here we assess the possibility of using phase-matched gratings to amplify the second-order diffracted beams obtained by nonlinear multiwave mixing. First we explain the concept, using expressions derived from the coupled-wave theory (CWT) of permanent gratings. A more detailed numerical examination is made that employs a finite-difference (FD) approximation of the paraxial-wave equation. Finally, experimental results are presented and assessed in the light of the modeling.

2. PHASE-MATCHED GRATING

As an approximation to the nonlinear scattering problem and to introduce the idea of phase matching, an analogous problem is first considered: that of diffraction from a lossless, permanent grating. It is assumed that the holographic grating has been written by two plane waves of equal intensity, intersecting at an angle θ, and is then read by a single probe beam incident at the Bragg angle $\theta_B = \theta/2$. The index distribution of the grating is given by

$$n(x) = n_0 + \Delta n \cos(Kx), \tag{2}$$

where n_0 is the background index and Δn is known as the modulation depth. The grating vector **K** is given by

$$K = \frac{2\pi}{\Lambda_g} = 2\pi \frac{2n_0 \sin(\theta/2)}{\lambda}, \tag{3}$$

where λ is the vacuum wavelength of the reading and writing beams and Λ_g is the grating period. This problem, schematically shown in Fig. 1, has been extensively examined by means of CWT.[8] It provides simple expressions for the variation of intensity with propagation distance for the various scattered beams. To a first approximation these expressions can also be used to represent the nonlinear process of four-wave mixing. The diffraction efficiency of a diffracted order is defined as the ratio of the intensity in that order to the intensity of the incident beam. The expressions associated with the first three scattered orders, to a good approximation, are as follows[8]:

$$\eta_p = \cos^2(\zeta), \tag{4}$$

$$\eta_b = \sin^2(\zeta), \tag{5}$$

$$\eta_s = \frac{\sin^2(\Omega\zeta)}{\Omega^2}, \tag{6}$$

where

$$\zeta = \frac{\pi(\Delta n)z}{\lambda \cos(\theta/2)}, \tag{7}$$

$$\Omega = \frac{\lambda^2}{{\Lambda_g}^2 n_0(\Delta n)}. \tag{8}$$

The second-order diffraction efficiency η_s can be written in terms of the phase difference Δk_z between the incident beam propagating at $\theta/2$ and the diffracted beam at $3\theta/2$:

$$\eta_s = \frac{\sin^2\left(\frac{\Delta k_z}{2} z\right)}{\Omega^2}, \tag{9}$$

where Δk_z is illustrated and defined in the reduced phase diagram shown in Fig. 2 as

$$\Delta k_z = k_p - k_s. \tag{10}$$

The reason for this relationship is as follows: A differential field element diffracted from the grating will always have a constant phase relationship with the writing beam. Whether it adds constructively or destructively will depend on the phase of the existing diffracted beam, and so the process depends on the phase difference between the generating and generated fields. If the differential field element were added only to increase the amplitude of the diffracted beam, namely, if it were added in phase, the resultant field should always be an increasing function of distance. This process could be achieved in practice by switching off the induced grating when the diffracted beam is out of phase with the pump. The waves are then allowed to propagate in a homogeneous medium until their phase difference is again zero. The grating is then reintroduced. Periodic repetition of this grating–buffer layer system forms a grating perpendicular to **K** with a grating vector of magnitude Δk_z that phase matches the second-order diffracted beam.

3. ANGULAR RESPONSE OF A PHASE-MATCHED GRATING

Consider a periodic system of lossless grating–buffer layer pairs, shown in Fig. 3, irradiated by a pump beam E_p incident at the Bragg angle for the grating layers. Within an individual grating, an elemental length Δz can be treated as a source radiating in the direction $3\theta/2$ with

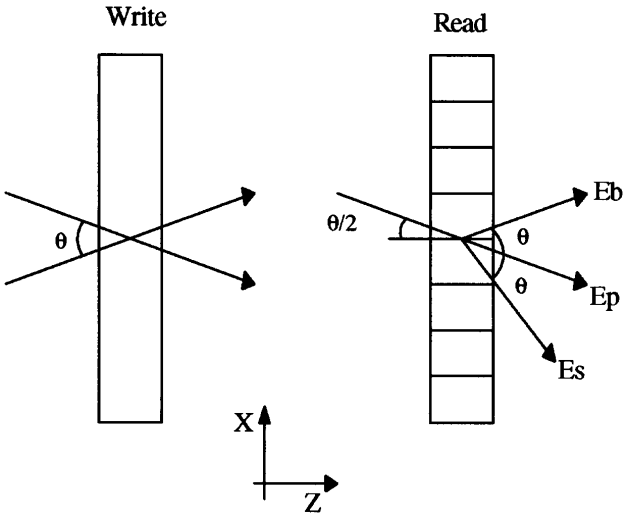

Fig. 1. Holographic phase grating written by two plane waves interferred at an angle θ and then read at the Bragg angle $\theta/2$.

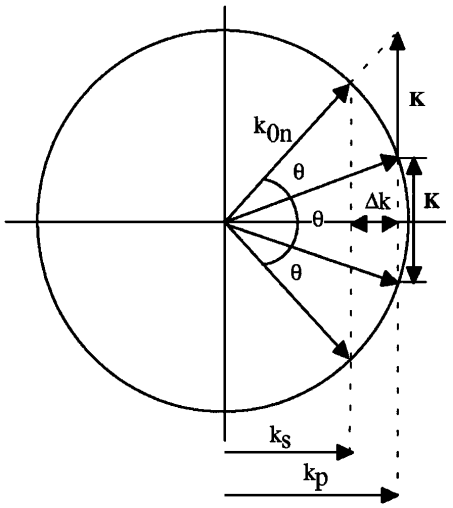

Fig. 2. Phase diagram for a grating being read at the Bragg angle of incidence.

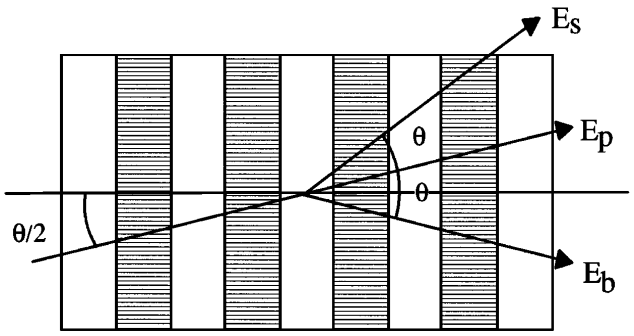

Fig. 3. A system of grating–buffer layers forms a grating of gratings that can phase match the signal E_s to the pump E_p.

an elemental field dE_s, whose magnitude per unit length is constant:

$$\frac{|dE_s|}{dz} = k_0 q |E_p| . \tag{11}$$

This assumes that the amplitude of the pump wave E_p is not depleted. The phase of the field element will depend only on the phase of the pump radiating in the $\theta/2$ direction. Integrating over the length of a grating layer gives the diffracted field as

$$E_s(L_g) = \frac{jqk_0}{\Delta k_z} |E_p| [\exp(-jk_p L_g) - \exp(jk_s L_g)], \tag{12}$$

where L_g is the length of a grating section. Propagation in the following buffer layer will then simply alter the phase according to the local refractive index. One can then track the evolution of the diffracted order through the system, taking into account local changes in refractive index. The diffraction efficiency for signal beam E_s will therefore be given by

$$\eta_s(z) = |E_s(z)|^2 / |E_p|^2 . \tag{13}$$

Assuming no losses and perfect phase matching, the total diffracted field after N nonlinear–linear layers will be $N[E_s(L_g)]$, and so the diffraction efficiency will be $N^2[\eta_s(L_g)]$. If the phase relationships were not preserved between layers[9] the intensities would add, giving a diffraction efficiency of $N[\eta_s(L_g)]$. The phase of the elemental field depends only on the phase of the writing beam, whereas the modulus, q, will be a function of the modulation depth of the refractive index. A comparison with results from a more rigorous CWT approach[8] shows that $q = \Delta n$. Obviously, for a permanent grating this is fixed, whereas in the nonlinear problem it will depend on the local intensity and nonlinearity. Using a representative value for q, one can use Eq. (12) to obtain the optimum grating and buffer layer thicknesses for a given crossing angle. Conversely, given layer thicknesses and indices, the diffraction efficiency can be deduced as a function of writing beam crossing angle θ. This is the angular response of the system and depends on the amplitude depth of the induced grating only through a scaling factor. Such an angular response is shown in Fig. 4. In this example four 1-mm grating layers of refractive index of 1.59 are separated by 1-mm glass-buffer layers of index 1.52. The operating wavelength was taken as $\lambda = 0.488\ \mu$m. The evolution of the diffraction efficiency with propagation distance is shown in Fig. 5 and represents the response at the optimum crossing angle $\theta = 1.1°$. As expected, for near-perfect phase matching the diffraction efficiency from the fourth nonlinear layer is 16 times greater than that obtained from one layer given the absence of loss.

4. FINITE-DIFFERENCE SIMULATION OF PERMANENT AND INDUCED GRATINGS

CWT has been extensively used to give a more rigorous analysis of FD four-wave mixing.[10–12] This has added greatly to the physical understanding of the process, but the use of a plane-wave approximation implies that effects that are due to finite beam sizes cannot be accounted for. For example, in highly nonlinear media beam distortions that are due to self-phase modulation can mask any mixing effects.[13] When phase-modulation terms are retained in plane-wave theories they simply alter phase-matching conditions, yet they are responsible for the more dominant self-focusing and -defocusing effects. Here, we simulated the nonlinear interaction, using a FD representation of the nonlinear paraxial-wave equation,[14] formally

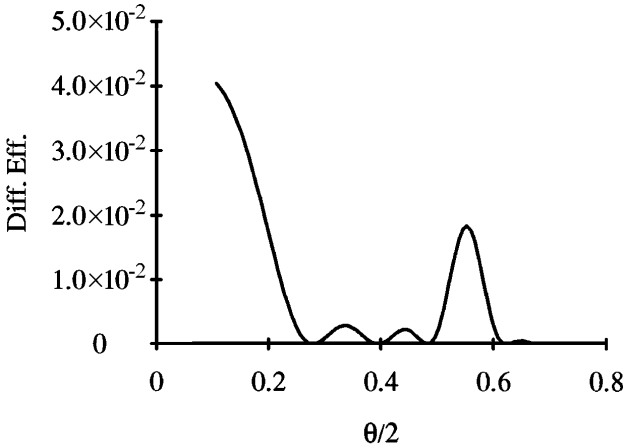

Fig. 4. Angular response of the second-order diffracted signal from a periodic grating–buffer layer system.

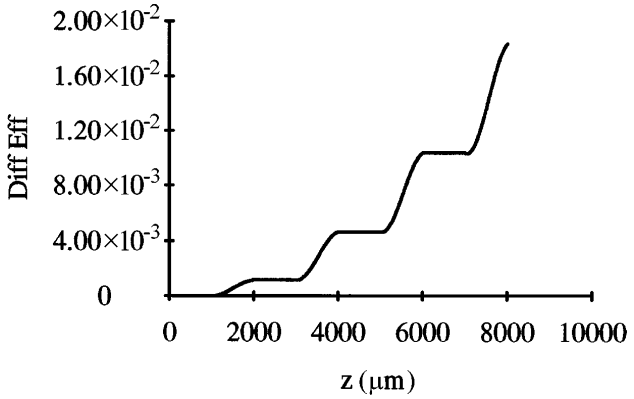

Fig. 5. Evolution of the second-order diffraction efficiency when the signal has been phase matched by the addition of an orthogonal periodicity.

equivalent to solving the nonlinear Schrödinger equation. This means that, to an approximation, a continuum of plane waves is considered, in contrast to the four or six waves treated in a numerical solution of the coupled-wave equations. Although the FD method has difficulties of its own, the problem to which it is being applied here is ideally suited to it. This is due largely to the fact that the spectral domain in which scattering takes place is well defined *a priori*. Boundary conditions, which often represent a problem with beam propagation techniques, are therefore easily applied. This is in contrast, for example, to the radiation modes of a waveguide induced by large refractive-index variations in the transverse direction. For the problem under consideration such variations do not exist. It is also assumed that for the near-normal propagation the index variations in the propagation direction do not induce substantial reflections.

The FD method, as applied to the paraxial-wave equation, is commonly used to analyze optical propagation. Although the calculations are made in the space domain, the presence of the different waves is clearly revealed by means of a conversion to the angular space domain by use of a fast Fourier transform. This is equivalent to using a lens to image a near-field distribution into a far-field distribution. Because of Parseval's theorem the squares of the Fourier amplitudes represent the intensities of the plane waves propagating at the different angles. The diffraction efficiencies can then be easily obtained.

As an example, and to demonstrate the validity of the program, scattering from a permanent grating is first considered. Here a comparison is presented between results obtained by CWT and a FD simulation of a permanent, lossless grating with the following parameters: $n_0 = 1.59$, $\Delta n = 8 \times 10^{-6}$, and $\Lambda_g = 21.35\ \mu$m. A Gaussian beam of radius $w_0 = 50\ \mu$m was considered incident at the Bragg angle in air of $\theta/2 = 0.655°$ for an operating wavelength of $\lambda = 0.488\ \mu$m. The incident beam amplitude profile is shown in Fig. 6. After the waves have propagated 6 mm, new waves have been generated that interfere producing the characteristic pattern shown in Fig. 7. The Fourier transform of this spatial distribution is shown on a logarithmic scale in Fig. 8. The pump and strong Bragg-diffracted waves are clearly present, propagating at 0.655° and −0.655°, respectively. The weak second diffracted order, referred to here as the signal, is also clearly seen, together with even weaker higher orders. The diffraction efficiencies can either be calculated by considering the square of the Fourier amplitudes at discrete angles or by integrating over the spectral bandwidth of the various propagating beams. The former alternative corresponds to CWT results, and the latter corresponds more closely to a detection measurement in the far field.

Comparisons of the diffraction efficiency for the Bragg beam, calculated by use of the CWT expression of Eq. (4) and the FD method, are shown in Figs. 9 and 10. The

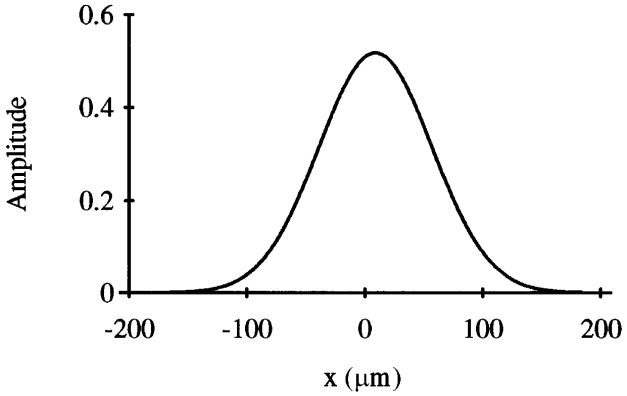

Fig. 6. Gaussian intensity distribution at the grating input.

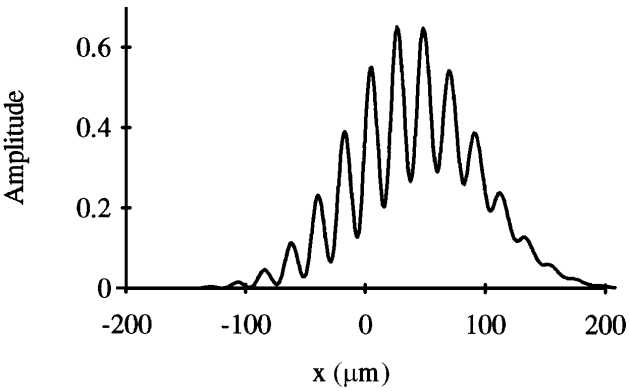

Fig. 7. Intensity distribution after the Gaussian input beam has propagated 6 mm in the grating at the Bragg angle of incidence.

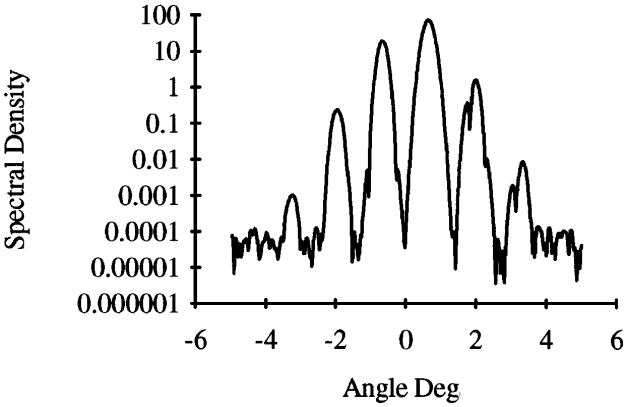

Fig. 8. A Fourier transform of the field having propagated 6 mm gives the amplitude distribution in angular space at that point. The pump and Bragg diffracted beams are clearly present, along with higher orders.

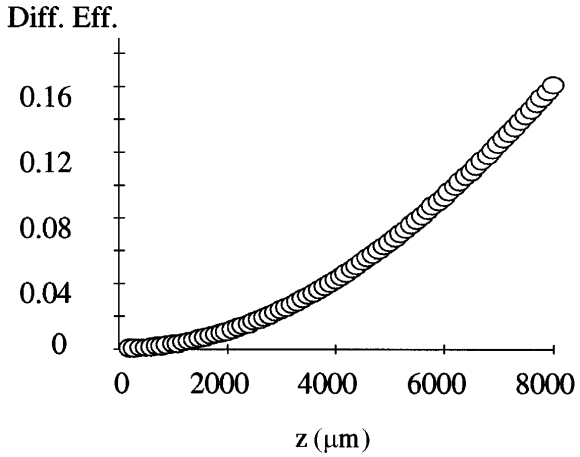

Fig. 9. Evolution and distance of the diffraction efficiency for a Bragg-diffracted beam. The results for CWT and FD BPM are coincident. The results from the FD simulation are indicated by circles and have been calculated at the discrete angle $\theta/2$.

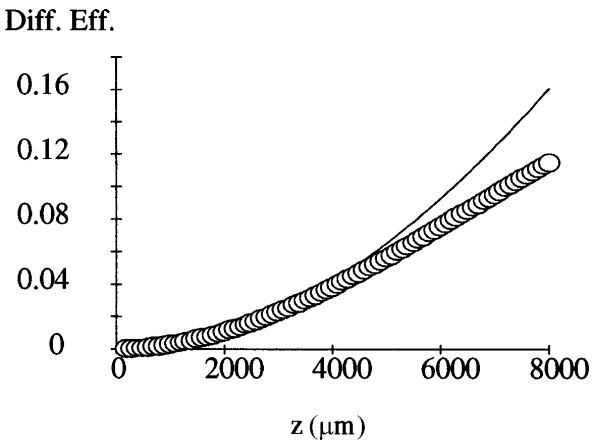

Fig. 10. Evolution with distance of the diffraction efficiency for a Bragg-diffracted beam. The solid curve corresponds to CWT, and circles to FD BPM. The results from the FD simulation have been calculated by integration over the spectral width of the diffracted order.

numerical analysis simulated propagation in a window 1.2 mm wide, using 1024 discretization points and a step size of 10 μm. For the FD method it is possible either to calculate the efficiency at a discrete angle or to integrate over the spectral width of the beam in question. When the discrete approximation is used, the comparison between CWT and the numerical simulation in Fig. 9 shows that the results are indistinguishable. For Fig. 10 the FD efficiency was calculated by integration. The point at which the results from the two methods diverge is related to the beam radius of the incident wave, wider beams being approximated more closely by a plane wave. A similar comparison is made in Figs. 11 and 12, where the diffraction efficiency of the second-order beam is considered. After the waves have propagated 8 mm there is clearly a phase difference between the CWT results and those obtained by discrete sampling of the FD angular spectrum. In Fig. 12 the differences are even more apparent; here the efficiency is calculated for the whole beam as opposed to for a single spectral element. Further analysis[15] shows that this discrepancy occurs because the perturbation theory neglects the changes of amplitude and phase of the pump beam; these changes slightly alter the period of oscillation of the diffracted beams. The finite bandwidth of the beam itself means that at any one position there is always some spectral element of the beam that is nonzero, and so the energy in the second-order beam does not periodically reach zero.

Having established confidence in the FD scheme to solve the linear paraxial-wave equation, we included a nonlinear response in a straightforward manner. In the absence of an experimental evidence for absorptive nonlinearity the following relationship was adopted as the model of the nonlinear process:

$$\hat{n} = \hat{n}_0 + n_2 I^p , \tag{14}$$

where the complex dc index n_0 allows for linear absorption and I is the local field intensity. The exponent p is introduced as a fitting parameter to account for nonideal

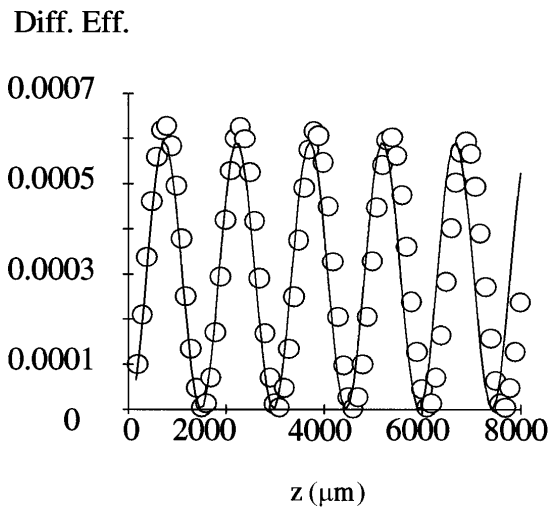

Fig. 11. Evolution with distance of the diffraction efficiency of the second-order beam. The solid curve corresponds to CWT, and the circles to FD BPM. The results from the FD simulation have been calculated at the discrete angle $3\theta/2$.

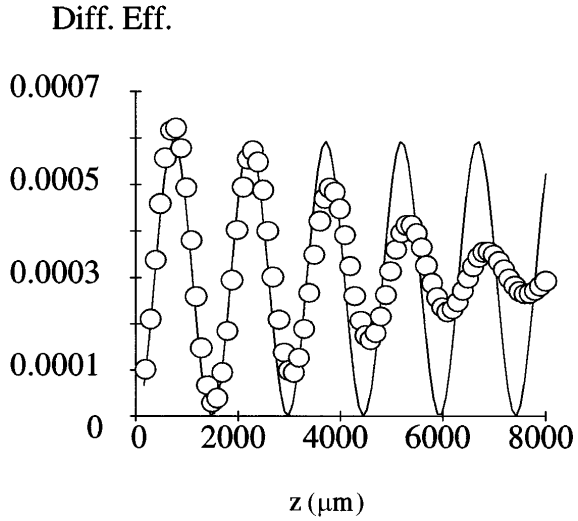

Fig. 12. Evolution with distance of the diffraction efficiency of the second-order beam. The solid curve corresponds to CWT, and the circles to FD BPM. The results from the FD simulation have been calculated by integration over the spectral width of the diffracted order.

Kerr-type behavior. The resulting FD program was then used to analyze the experimental results obtained from phase-matched grating (PMG) nonlinear devices.

5. EXPERIMENTAL RESULTS

A. Sample Preparation and Experimental Setup

The concept of PMG's was experimentally investigated with the use of samples consisting of nonlinear layers of dye-doped epoxy resin sandwiched by 1-mm linear buffer layers of glass microscope slides. We formed the nonlinear layers by cutting holes in identical glass slides and filling the 1-mm-thick cavity with the resin. The epoxy, Araldite MY 757, was doped with a 1.5-g/L solution of Alizarin Yellow in ethanol. This dye is characterized by a strong, thermal nonlinearity in the blue wavelength. The doping level was chosen as a trade-off between nonlinearity and absorption.

We performed all the experiments, linear and nonlinear, with a cw Ar:Kr laser, using the strongest line, $\lambda = 0.488\ \mu$m. The refractive indices of the glass, n_g and of the epoxy films, n_f, were measured by standard techniques to be $n_g = 1.52$ and $n_f = 1.59$. We obtained the linear absorption losses by illuminating each sample with a 0.5-mW input beam and then detecting the transmitted power. Assuming no losses in the glass, the linear absorption in the epoxy films was measured as $\alpha = 17$ dB/cm.

Three samples were fabricated: S1, S2, and S4. Sample S1 consisted of a single grating period and is illustrated in Fig. 13. Samples S2 and S4 represented two and four grating periods, respectively. The nonlinear experiments were performed with a standard FDFWM setup[2] shown in Fig. 14. A 50/50 cube beam splitter and mirrors were adjusted to produce a pair of beams propagating in the same plane that interfere *after* the focal plane of the lens, L. The crossing angle is determined by the focal length of L and the beam separation. This arrangement produces beams that are diverging as they overlap. This has the important advantage that the resulting interference region is long enough to contain the samples and wide enough to include a reasonable number of grating periods off which the incident beams might diffract. The angular divergence of the beams themselves also relaxes the tolerance on obtaining the required crossing angle. The period of the induced grating, however, will not be uniquely defined over the overlap region. This feature is accounted for by use of the FD representation of the interaction.

Diffracted beams were monitored with photodiode P connected to an oscilloscope. A lens of focal length 33 cm was chosen. We measured the separate beam profiles and their combined interference pattern as a function of position by scanning the intensity profiles with a slit mounted upon a photodiode. An example is shown in Fig. 15, where the crossing beams have been recorded just before they fully overlap. The experimentally measured points have been fitted with Gaussian profiles. The resulting interference pattern is given in Fig. 16. Another interference pattern, measured after the beams have propagated a further 7 mm and have crossed over, is shown in Fig. 17. A comparison between these plots shows the extent of the beam divergence. This is implied not only by the increased width of the profiles but also by the change in periodicity of the interference patterns. This is caused by the phase curvature of the beam wave fronts. The consequence of this in a nonlinear medium would be a diffraction grating whose periodicity would be chirped in the propagation direction. By careful fitting, assuming Gaussian field profiles, it was possible to deduce from such intensity measurements the following parameter values: minimum beam radius $w_0 = 50\ \mu$m and crossing angle $\theta = 1.31°$ in air.

The resulting interference region is schematically represented in Fig. 18, where the minimum beam waists occur on the $z = 0$ axis. It is expected that the response

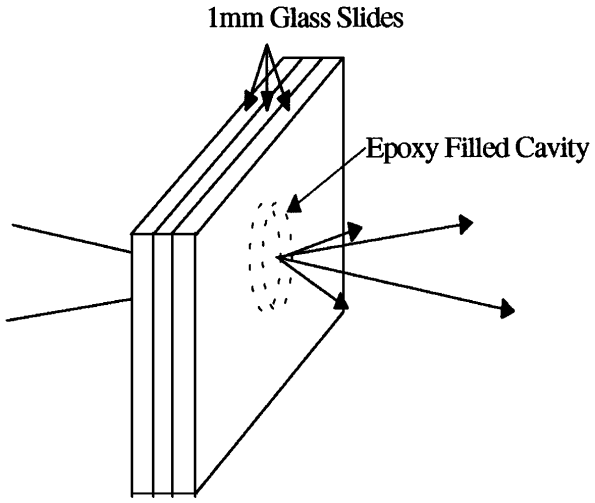

Fig. 13. Sample S1. A single nonlinear epoxy resin layer sandwiched between two glass slides.

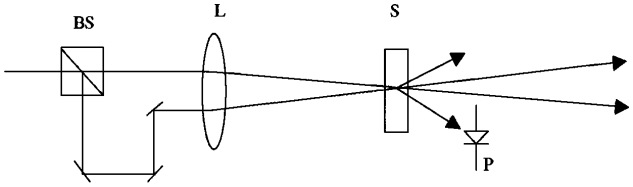

Fig. 14. Experimental setup for degenerate forward four-wave mixing: BS, beam splitter; L, lens; S, sample; P, photodiode.

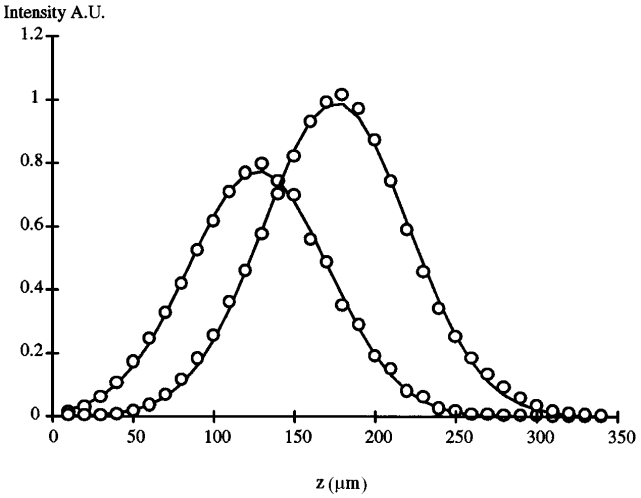

Fig. 15. Separately measured input beam intensities fitted with Gaussian profiles.

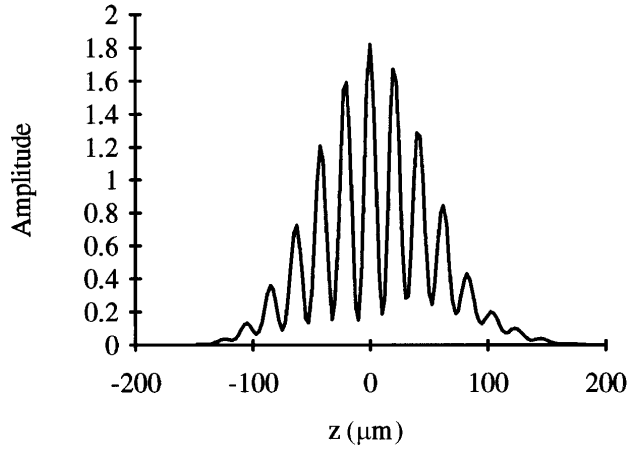

Fig. 16. Resulting interference pattern produced by the two Gaussian beams.

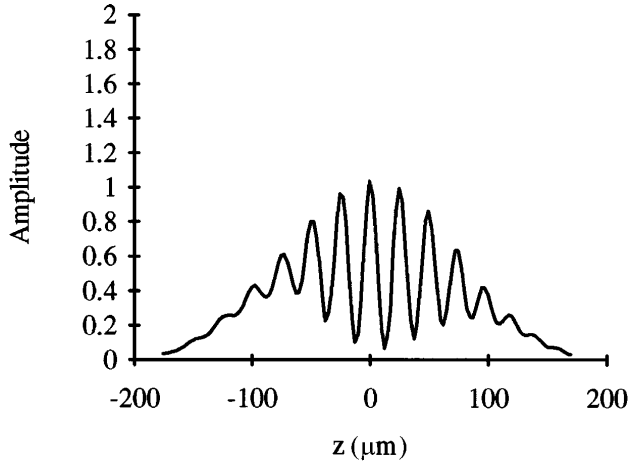

Fig. 17. Interference pattern after the beams have propagated a further 6 mm.

of a sample will depend on its position within this region, partly as a function of the number of interference fringes and partly as a function of their spacing. It is these factors that cannot be accounted for in a plane-wave theory.

B. Material Characterization

A number of experiments were performed to establish the nature of the nonlinearity. First, we measured the step response by monitoring the diffracted beam intensity induced by the samples after the pump beams had been switched on. The nonlinear mechanism is slow and thermal in origin. The steady state corresponds to the formation of a permanent grating, the definition of which degrades by diffusion processes. As a result, throughout the subsequent experiments the maximum dynamical response was measured to represent the nonlinear effect.

In Fig. 19 the diffracted power is plotted as a function of the pump power. A simple best fit, using a power law, shows that the behavior is characterized by an exponent of 1.3. This result was obtained for various crossing angles and is in contrast to an ideal Kerr response, which would exhibit an exact cubic dependency. The departure from the ideal behavior is not fully understood. According to Fig. 19, the parameter p in Eq. (14), which accounts for the nonlinear effects in the FD simulation, is, to a good approximation, given by $p = 0.15$. Usually the nonlinear index n_2 is treated as a physical constant. Here, because Eq. (14) is phenomenological in origin, it is best treated as a fitting parameter.

C. PMG Measurements

The experimental results concerning the PMG are reported in Table 1, where the diffraction efficiencies for the three samples are listed. For each sample we maximized the diffraction efficiency by translating it within the interference region. This may considered akin to sampling different spectral components of the beams. At the front of the overlap region only components with a larger than average crossing angle are interfering, whereas at the end of the region only the narrow crossing angle components are present. The average diffraction efficiency value, resulting from many measurements made at a constant input power of 0.5 mW per beam, has been quoted for each device. Because the intensities of the input beams were not equal, an asymmetry has been induced in the efficiencies of the signal beams. Here results for the stronger diffracted beam are given.

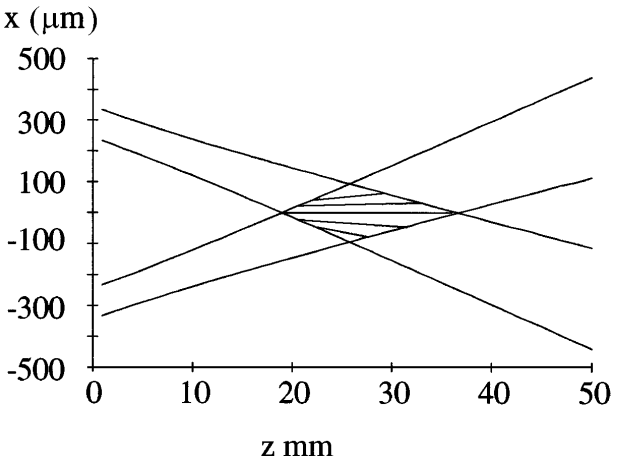

Fig. 18. Schematic of the interference region produced by diverging Gaussian beams.

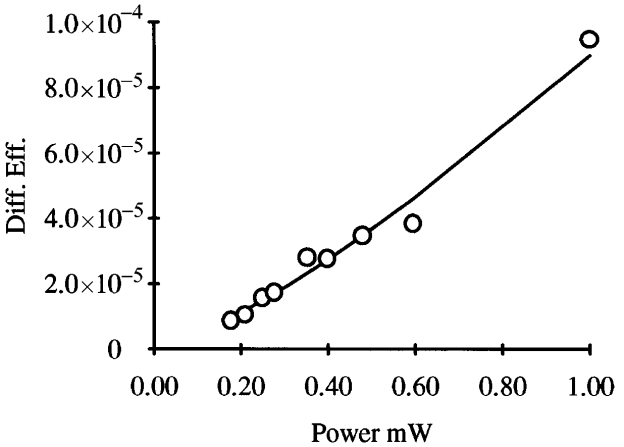

Fig. 19. Dependence of the second-order diffraction efficiency on input power. The experimental data have been fitted with a simple power law whose coefficient is 1.3. Had the response been governed by the ideal Kerr effect the dependency would have been exactly cubic.

Table 1. Measured Diffraction Efficiency for Samples S1, S2, and S3

Sample	Diffraction Efficiency ($\times 10^{-5}$)
S1	1.6
S2	2.6
S4	3.5

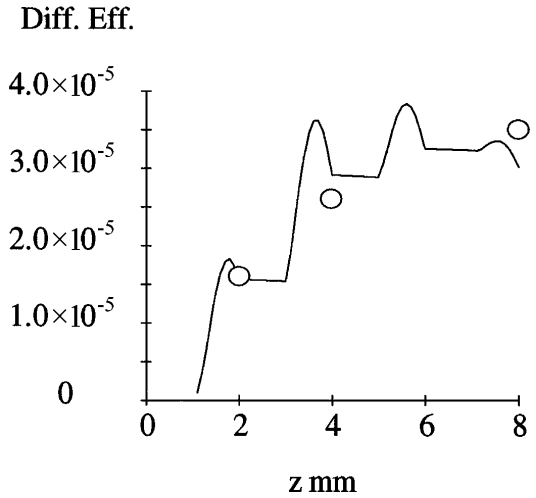

Fig. 20. Evolution with propagation distance of the second-order diffraction efficiency calculated for sample S4. Experimental measurements are also indicated, with circles corresponding to measurements on samples S1, S2, and S4.

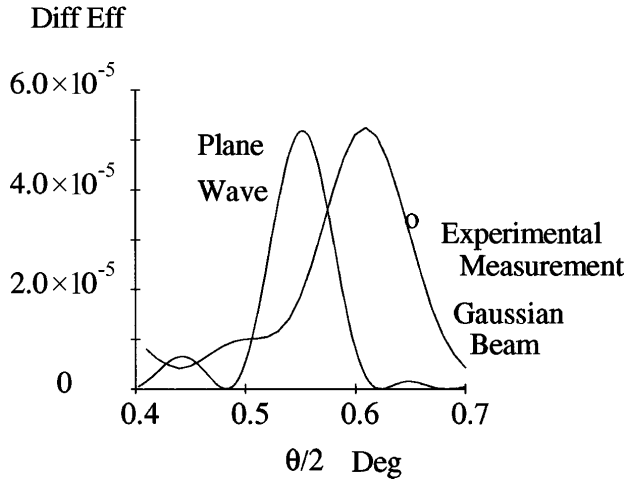

Fig. 21. Angular response of S4 calculated by use of the FD simulation, assuming the Gaussian beam parameters measured in the experiment. For comparison the results from plane-wave theory have also been indicated.

D. Analysis of Experimental Results

We simulated the performance of the PMG, using the FD program, given the experimental input conditions. The stronger of the two pump beams was normalized to a maximum intensity of 1.0 at the minimum beam waist. The ratio of the pump beam field intensities was measured to be 0.79. We then calculated the diffraction efficiency as a function of propagation distance in S4 by integrating over the spectral width of the new beam. The optimal position of the sample within the chirped interference region was found and used throughout. This procedure mimicked that used in the experiment. The evolution of the stronger diffracted wave is shown in Fig. 20. Also indicated are the experimental values obtained for S1, S2, and S4. We obtained the calculated curve by varying the value n_2 to give close agreement for the measured diffraction efficiency from S1. The nonlinear index thus found was $n_2 = 1.2 \times 10^{-5}$. Given the normalized units of the field amplitudes, this gave a maximum induced index modulation $[\Delta n/2 = n_2(I_{\max})^{0.15}]$ of approximately $1.3\ 10^{-5}$. The upward trend of the experimental results, despite high absorptive losses, and the correspondence with the theoretical predictions indicate that phase matching has been successfully achieved. We reconfirmed this conclusion by measuring the diffracted signal from a sample with a single nonlinear layer with a thickness twice that used in S1. This corresponds to an exact phase mismatch, and accordingly the signal, if any, was below the measurable threshold of the experiment.

Numerical simulations have confirmed, however, that the experimental conditions were not optimal. The angular response of S4 is shown in Fig. 21, assuming the nonzero beam divergence measured in the experiments. Also shown is the response calculated by the plane-wave theory of Eq. (12). This would correspond more closely to the foci of two, broad-area pump beams that are overlapping. The phase curvature present in the crossing beams after focus has shifted the resonance curve to a larger angle and made it broader. This slightly relaxes the tolerance required for the angular control in the experiment. To obtain the maximum output efficiency, twice that of the one observed, a control of θ to within 0.19 would be required. This is beyond the capabilities of the current experimental setup.

The narrow crossing angle to produce phase matching in the three fabricated samples was determined by the thickness of the linear and nonlinear layers. To obtain phase matching at larger angles one must make an appropriate choice of layer thickness. For example, under the plane-wave approximation, glass and epoxy layers of 304 and 318 μm, respectively, would move the resonance to 2°. The advantage of operating at larger angles will be offset, however, by a reduction in the length over which the beams interact. This could, of course, be compensated for by use of wider, more powerful beams.

6. CONCLUSIONS

Layered systems of glass and dye-doped epoxy resin have been used to demonstrate, for the first time to the authors' knowledge, phase matching for FD four-wave mixing. The use of focused beams meant that a plane wave interaction could not be assumed. The experimental results were then successfully explained by use of a FD analysis of the finite-sized beam interactions in a nonlinear medium. The results successfully demonstrate the ability of PMG's to enhance the efficiency of FD four-wave mixing. PMG's could be conveniently be used in all-optical devices. In particular, high diffraction efficiencies might still be obtained in an integrated waveguide in which the chip length prevents the use of narrow crossing angles. They could also be employed in material systems that are intrinsically short, such as liquid crystals and multiple quantum wells.

ACKNOWLEDGMENTS

This research was carried out under the European collaborative project RACE 2012 and the Italian Project on Telecommunications. Q. Li acknowledges the support of the International Center for Theoretical Physics Programme for Training and Research in Italian Laboratories, Trieste, Italy.

REFERENCES

1. I. C. Khoo and T. H. Liu, "Theory and experiments on multiwave-mixing-mediated probe-beam amplification," Phys. Rev. A **39,** 4036 (1989).
2. P. Horan, W. Blau, H. Byrne, and P. Berglund, "Simple setup for rapid testing of third-order nonlinear optical material," Appl. Opt. **29,** 31 (1990).
3. D. L. Staebler and J. J. Amodei, "Coupled-wave analysis of holographic storage in $LiNbO_3$," J. Appl. Phys. **43,** 1042 (1972).
4. M. Zha, D. Fluck, P. Gunter, M. Fleuster, and Ch. Buchal, "Two-wave mixing in photorefractive ion-implanted $KNbO_3$ planar waveguides at visible and near-infrared wavelengths," Opt. Lett. **18,** 577 (1993).
5. B. Ya. Zel'dovich, D. I. Mirovitskii, N. V. Rostovtseva, and O. B. Serov, "Characteristics of two-layer phase holograms," Sov. J. Quantum Electron. **14,** 364 (1984).
6. A. Granger, L. Song, and R. A. Lessard, "Multiple beam generation using a stratified volume holographic grating," Appl. Opt. **32,** 2534 (1993).
7. G. P. Nordin, R. V. Johnson, and A. R. Tanguay, Jr., "Diffraction properties of stratified volume holographic optical elements," J. Opt. Soc. Am. **9,** 2206 (1992).
8. L. Solymar and D. J. Cooke, *Volume Holography and Volume Gratings* (Academic, Orlando, Fla., 1981), p. 130.
9. D. J. De Bitetto, "On the intensifying property of a pile-of-gratings," Appl. Opt. **9,** 59 (1970).
10. P. Yeh, "Exact solution of a nonlinear model of two-wave mixing in Kerr media," J. Opt. Soc. Am. B **3,** 747 (1986).
11. T.-H. Liu and I.-C. Khoo, "Probe beam amplification via degenerate optical wave mixing in a Kerr medium," IEEE J. Quantum Electron. **QE-23,** 2020 (1987).
12. F. Sanchez, "Two-wave mixing in thin nonlinear local-response media: a simple theoretical model," J. Opt. Soc. Am. B **9,** 2196 (1992).
13. I. V. Tomov and P. M. Rentzepis, "Effect of thermal self-defocusing of degenerate four wave mixing in absorbing media," Appl. Phys. Lett. **29,** 31 (1994).
14. R. Accornero, M. Artiglia, G. Coppa, P. Di Vita, G. Lapenta, M. Potenza, and P. Ravetto, "Finite difference methods for the analysis of integrated optical waveguides," Electron. Lett. **26,** 1959 (1990).
15. D. Yevick and L. Thylén, "Analysis of gratings by the beam-propagation method," J. Opt. Soc. Am. **72,** 1084 (1982).